STRESS-STRAIN BEHAVIOUR, DISSIPATION AND INSTABILITY OF MEDIUM-CARBON STEEL

Jiri Kliber, Vojtěch Ševčák, Petr Opěla

VSB- Technical University of Ostrava, Faculty of Materials Science and Technology, 17. Listopadu 15/2172, Ostrava – Poruba, 708 33, Czech Republic
E-mail: jiri.kliber@vsb.cz

Received 31 October 2019
Accepted 16 December 2019

ABSTRACT

Metallic materials that have exceeded elastic deformation deform plastically with hardening. The method of determining properties is operated by means of stress-strain curves. Plastometric tests on Gleeble were used, which always allow one of the three thermomechanical mechanical parameters to remain constant, even in this case. The aims of the paper are two: namely to describe mathematically the course of these stress-strain curves and then to derive the values of energy dissipation and plastic deformation instability. This dataset was acquired via series of uniaxial hot compression tests in the temperature range of 1173 K - 1553 K and the strain rate range of 0.1 s^{-1} - 100 s^{-1}. The analysis used sinh relation for determination of activation energy and other constants, which was based on experimentally measured values of peak, i.e. maximum stress, with comparison of measured and calculated values. Subsequently, process maps are compiled using the energy dissipation efficiency η and the plastic deformation instability criterion ξ, and these two parameters are also interpreted together as the criteria of formability at high temperatures.

Keywords: medium-carbon steel, stress-strain, dissipation, instability.

INTRODUCTION

The method proposed in the 1980s to describe the response of material to process parameter change Dynamic Material Modeling (DMM) has been carefully elaborated by Prasad et al. It is a continuous model based on thermodynamic principles by which the areas of material flow instability are determined. It is also able to show the transitions between plastic deformation of materials and the formation of thermodynamically unstable dissipative microstructure. DMM focuses on the localization of dynamic recrystallization and describes the deformation behavior of the material even at high strain rates at which dynamic recovery processes can take place. The equations used in DMM describe stress response in plastic flow dependent on macroscopic forming parameters such as strain rate and temperature. Using these equations, it is possible to determine the proportions of the dissipated energy stored in the mechanical part, i.e. induced heat, and also in metallurgical processes [1 - 8].

In forming, energy dissipation is characterized by a dimensionless quantity, named as energy dissipation efficiency η. It is a key element that uses Dynamic Material Modeling (DMM) [9].

The total energy P absorbed by the body during deformation is composed of two parts, the first part being energy G, which represents the energy input dissipated by the material, much of which is converted to heat. The second part presents supplement J, which represents the energy dissipated due to metallurgical changes in dynamic recrystallization, dynamic recovery, nucleation, crack growth and other processes, and therefore is a criterion characterizing the dynamic response of a material [1]. The total energy can thus be expressed by the following equation (1):

$$P = G + J \quad (1)$$

where: P - total energy absorbed by the body during deformation [J], G - energy dissipated due to plastic deformation [J], J - energy dissipated due to metallurgical changes [J]. The main variables describing process maps are strain, stress, strain rate. Thanks to these variables,

the formula above can be further described [1], resulting in the resulting equation for J [10 - 13]

The maximum value of J occurs when m = 1 [3]. Then we get the equation:

$$J_{max} = \frac{\sigma \, . \, \dot{\varepsilon}}{2} \tag{2}$$

The coefficient of the plastic material flow sensitivity to the strain rate describes the distribution of total energy P between the components G and J. It is a function of the strain rate. The ideal value of the coefficient m is 1. This coefficient is very important for the creation of process maps and can be expressed as follows [11]:

$$m = \frac{dJ}{dG} = \frac{\dot{e}\, d\sigma}{\sigma\, d\dot{e}} = \frac{d\, ln\, \sigma}{d\, ln \dot{e}} \tag{3}$$

Knowing the equations for calculating the values of J and J_{max}, we can determine the dimensionless parameter η (a dissipation efficiency), which is very important for creating process maps. The dissipation efficiency can thus be expressed as follows [12, 13]:

$$\eta = \frac{J}{Jmax} = \frac{2m}{m+1} \tag{4}$$

If we multiply the results by 100, we get the percentages in which efficiency is usually reported.

Another important parameter is the plastic instability parameter, by means of which it is possible to determine the areas in which the material forming is stable and the areas in which the material can break during forming, especially in forming under unsuitable conditions such as higher friction coefficient. This parameter can be expressed by the following equation (5):

$$\xi = \frac{\partial\, ln\left(\frac{m}{m+1}\right)}{\partial\, ln\, \dot{e}} + m < 0 \tag{5}$$

The lower the plastic instability parameter, the less stable is the region. Negative values indicate areas of instability [14].

EXPERIMENTAL

Strain rates from 0.1 s^{-1} to 100 s^{-1} were used for the plastometric tests and temperatures ranging from 900°C to 1280°C. The data are then used to construct stress - strain graphs. As an example of a stress-strain curve for a strain rate of 1 s^{-1} and different temperatures is the Fig. 1.

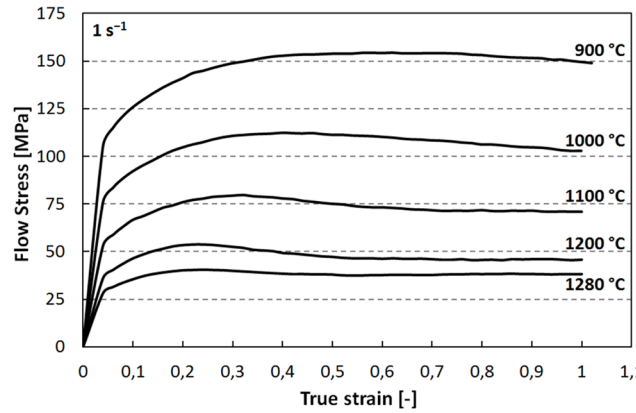

Fig. 1. Example of stress-strain curves for strain rate 1 s^{-1}.

STRESS-STRAIN BEHAVIOUR

Calculation of the peak stress

One of the goals of this work is the mathematical evaluation of peak stress and strain and the subsequent compilation of a complete mathematical description of this curve. The correctness of the future solution lies in the comparison of experimental values of peak stress σ_{pex} with calculated $\sigma_{pca\ 1}$ and the same for peak deformation ε_{pex} and ε_{pca}. Since the dependence of the peak values are an exponential functions of temperatures, this fact will be used in mathematics and the v values of $\sigma_{pca\ 2}$ were examined.

The procedure consists in determining peak points on the actual course of the curves obtained on the plastometer. We continue with the regression and equations described below, the constant α is calculated. Subsequent regression analyzes using the equation:

$$\alpha = \frac{\beta}{n_t} \tag{6}$$

For the highest temperatures we use the relation $\dot{\varepsilon} = f\left(\sigma_{pex}\right)$ in the power form with obtaining the constant n; furthermore for the lowest temperatures the relation in the form $\dot{\varepsilon} = f\ exp(\sigma_{pex})$ with obtaining the constant β; and then at $\alpha = \frac{\beta}{n_t}$, the constant α is calculated. Subsequent regression analyzes using the equation (7):

$$\ln \dot{\varepsilon} = f\left[\ln \sinh(\alpha \cdot \sigma_{pex})\right] \tag{7}$$

Table 1. Some experimental and calculated results.

T	T [K]	$\dot{\varepsilon}$	σ_{pex}	$\sigma_{pca\,1}$	$\sigma_{pca\,2}$	ε_{pex}	ε_{pca}
1280	1553	0,01		16,04	13,75		0,05
1280	1553,00	0,10	21,10	26,07	22,71	0,12	0,10
1280	1553,00	1,00	40,40	42,39	37,49	0,22	0,17
1280	1553,00	10,00	61,10	68,90	61,91	0,30	0,31
1280	1553,00	100,00	100,60	111,98	102,23	0,48	0,54
1280	1553,00	500,00		156,26	145,14		0,81
1200	1473,00	0,01		20,28	19,88		0,06
1200	1473,00	0,10	31,3	32,97	32,09	0,14	0,11
1200	1473,00	1,00	53,8	53,60	51,81	0,24	0,20
1200	1473,00	10,00	83,6	87,13	83,64	0,36	0,35
1200	1473,00	100,00	133,4	141,27	135,02	0,56	0,62
1200	1473,00	500,00		190,67	188,71		0,93
1100	1373,00	0,01		28,26	33,65		0,08
1100	1373,00	0,10	48,3	45,94	50,33	0,18	0,14
1100	1373,00	1,00	79,4	74,69	75,29	0,31	0,24
1100	1373,00	10,00	114,6	121,34	112,63	0,51	0,44
1100	1373,00	100,00	163,6	189,59	168,48	0,62	0,77
1100	1373,00	500,00		227,50	223,25		1,16
1000	1273,00	0,01		41,49	51,00		0,11
1000	1273,00	0,10	72,8	67,45	74,22	0,26	0,19
1000	1273,00	1,00	112,40	109,62	108,03	0,40	0,34
1000	1273,00	10,00	153,90	174,88	157,23	0,68	0,60
1000	1273,00	100,00	229,10	231,25	228,85	0,81	1,07
1000	1273,00	500,00		254,51	297,49		1,60
900	1173,00	0,01		65,04	85,04		0,18
900	1173,00	0,10	113,10	105,71	114,10	0,40	0,32
900	1173,00	1,00	154,40	169,44	153,11	0,62	0,57
900	1173,00	10,00	207,50	228,18	205,45	0,94	1,02
900	1173,00	100,00	273,10	260,59	275,68	0,98	1,81
900	1173,00	500,00		276,63	338,58		2,71

leads to the intersection constants with the vertical z – axis A_1 *to* $A_n = f\left(\frac{1}{T}\right)$ and to the equation (8).

$$\ln\dot{\varepsilon} + \frac{Q}{RT} = f\left[\ln\sinh\left(\alpha\cdot\sigma_{pex}\right)\right] \tag{8}$$

The calculated constants A_1 to A_n substituted for the equation $\left(\frac{1}{T}\right)$ to determine the negative slope *S*, where the activation energy is *Q* (J/mol) of the process and can be found by simple calculation according to $Q = -R\cdot S$ (R is the gas constant, R = 8,314 (J/(mol·K)). Using the equation (9) we construct a single line from the already known values and then determine the slope *n* and the intersection with the y-axis from which we calculate the constant *A*.

$$\ln\dot{\varepsilon} + \frac{Q}{RT} = f\left[\ln\sinh\left(\alpha\cdot\sigma_{pex}\right)\right] \tag{9}$$

We will build the final relationship:

$$\dot{\varepsilon} = A\exp\left(\frac{-Q}{RT}\right)\sinh\left(\alpha\cdot\sigma_{pex}\right)^n \tag{10}$$

By adjusting equation (11) using the obtained constants $A = 8{,}702\text{E}11$; $Q = 264410$; $\alpha = 0.00537$; $n = 4.74$ we arrive at an analytical expression of the maximum (peak) calculated stress as a function of temperature and strain rate, namely:

$$\sigma_{pca} = \frac{1}{\alpha}\arg\sinh\left[\frac{\dot{\varepsilon}\exp\left(\frac{Q}{RT}\right)}{A}\right]^{\frac{1}{n}} \tag{11}$$

In the literature it is possible to find another notation of this equation, where, $\dot{\varepsilon}\exp\left(\frac{Q}{RT}\right)=Z$ which represents the Zener-Hollomon parameter [15 - 18]. The resulting equation (11) allows both to check and compare the measured experimental values of peak deformations σ_{pex} with the newly calculated calculated $\sigma_{pca\ 1}$, but also to try to extend the values by interpolation to one lower and one higher strain rate. In the well-arranged table, the rows with interpolated results are gray and are listed in the special columns. Since the stress is generally the Arhenius exponential dependence on the temperature in the monophasic region, the calculated values of $\sigma_{pca\ 2}$ are also shown in the table column. Therefore, these values were not used for subsequent energy dissipation and instability.

Calculation of the peak deformation

We use the parametric equation model and the hyperbolic sinus model. This model is based on proven experience in solving theoretical courses in the analysis of plastic deformation driven by dynamic recovery by non-conservative dislocation movement (Barett's model). In principle, the limit deformation is dependent on temperature and strain rate [15 - 18]. We start by building linear regression eqs. (12) and (13), (where there is a peak deformation ε_{pex}) for individual temperatures and determine their slope, which we denote k_1 to k_n and then we calculate the slope of the average slope k, where its value reachs $k = 0{,}204$

$$\ln\varepsilon_{pex}=f\left(\ln\dot{\varepsilon}\right) \tag{12}$$

Then we use equation (13)

$$\sinh\left(\ln\varepsilon_{pex}-k\ln\dot{\varepsilon}\right)=f\left(\frac{1}{T}\right) \tag{13}$$

and graphically and mathematically we determine the slope, which we denote as X and the intersection with the y-axis, which we denote by the letter Y and construct the final relation (X = 10 758; Y = -9,756)

$$\varepsilon_{pca}=\dot{\varepsilon}^{\,k}\exp\left[\arg\sinh\left(Y+\frac{X}{T}\right)\right] \tag{14}$$

After substituting all calculated values into the final relation (14) we get the calculated peak deformation values, which are compared with the experimental values. If these were stress-strain curves for materials where a rapid stress drop occurs after the peak deformation is reached and the drop is sustained, the resulting equation (15) in the form that it describes, based on previous knowledge of the calculated peak stress σ_{pca} and calculated peak strain ε_{pca} complex expression of material characteristics as a function of temperature T and strain rate $\dot{\varepsilon}$ [15 - 20].

$$\sigma_{ca}=\sigma_{pca}\cdot\frac{\varepsilon}{\varepsilon_{pca}}\cdot\exp\left(1-\frac{\varepsilon}{\varepsilon_{pca}}\right)^{c} \tag{15}$$

The investigated steel does not meet this requirement, it even appears that at the lowest temperature of 900°C and a strain rate of 100 s^{-1} the peak stress σ_{pex} is reached, therefore we did not use this equation (15) further.

DISSIPATION AND INSTABILITY

The principles of the Dynamic Material Model were used to construct energy dissipation maps [21 - 26]. To obtain the energy dissipation factor η the following steps were performed: from the stress-strain dependence, three deformations are selected, namely 0.2; 0.5 and 0.8 and for these sizes the values of deformation resistance for individual temperature of 900°C to 1280°C and strain rate of 0.1; 1; 10 and 100 s^{-1} are subtracted. The stress-strain rate obtained in this way are converted to the stress-logarithm of the strain rate and then the logarithm of the strain rate $\Delta\log\dot{\varepsilon}$. For these and other calculations an overall table has been compiled, as an example we show only the result of the strain 0,5 and temperature 1000°C. To calculate the coefficient of deformation sensitivity m it is necessary to calculate the logarithm of stress ($\log\sigma$) and difference of logarithm of stress ($\Delta\log\sigma$) and the logarithm difference of stress ($\Delta\log\sigma$) and then dissipation η.

Finally, it is necessary to calculate the plastic insta-

Table 2. Results of dissipation and instability for strain 0,5.

T[°C]	ln $\dot{\varepsilon}$	m	η	ξ
1000	-2,25	0,20	34	-0,055
1000	0,06	0,13	24	0,075
1000	2,37	0,14	25	0,254
1000	4,53	0,23	37	0,465

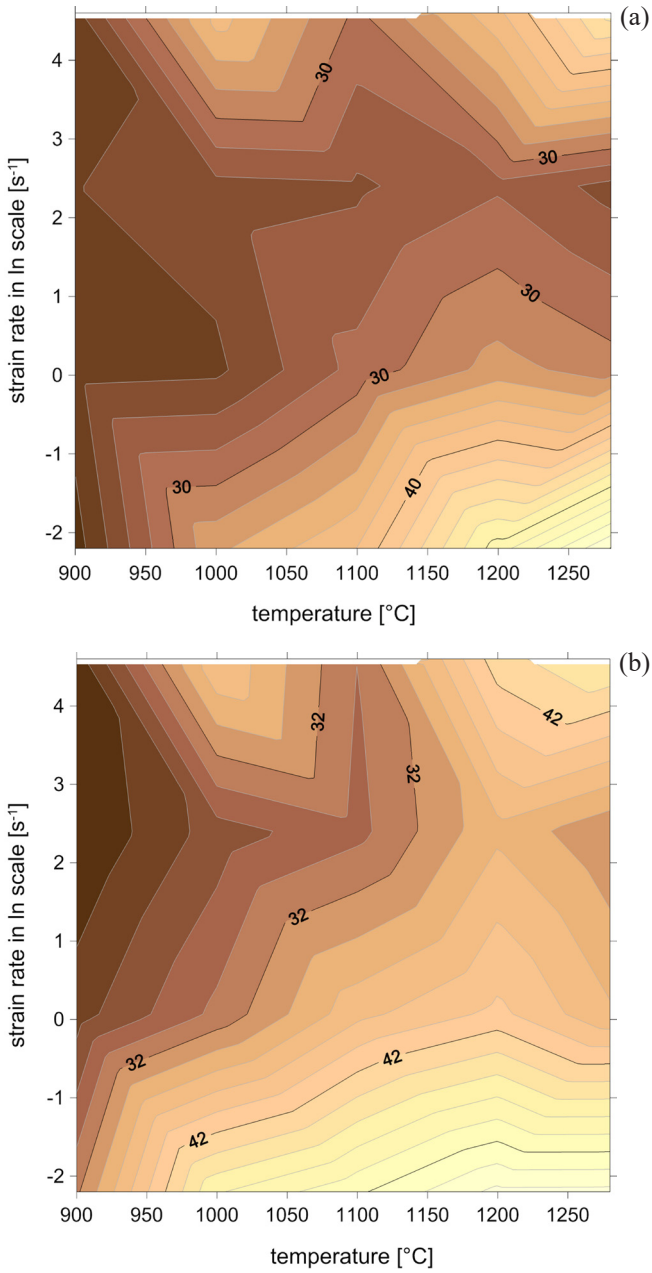

Fig. 2. Dissipation at strain 0,5 (a) and 0,8 (b).

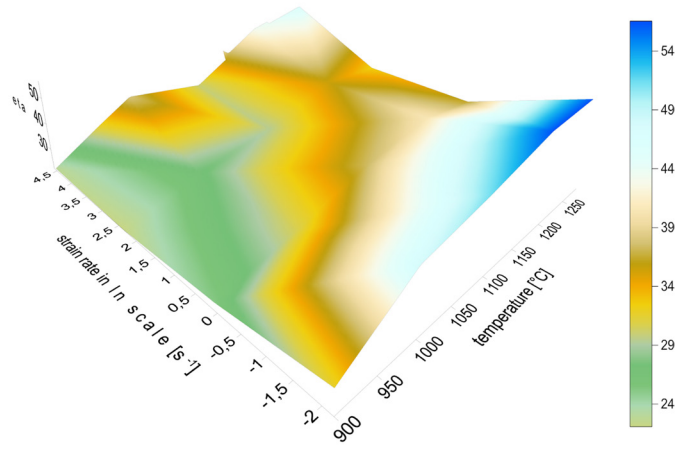

Fig. 3. Surface graph for dissipation at strain 0,8.

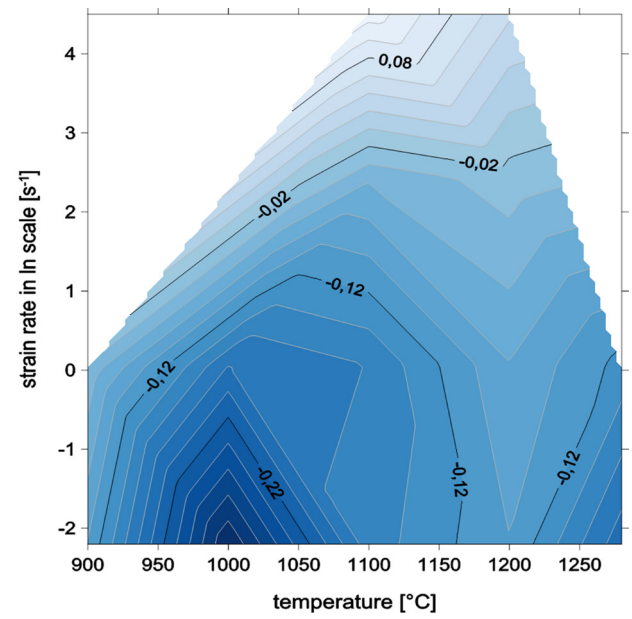

Fig 4. Instability at strain 0,5.

bility parameter ξ, which can be used to determine the areas in which the material deformation is stable and the areas in which the material can break during forming and we used only negative values according to equation (4) [27 - 31]. The results were processed in Golden Surfer 13.0. We present examples of results for dissipation at all temperatures and strain rates for deformation 0,2 and 0,8 from the whole range of isocurves and at the same time the graph in the space for deformation 0,8. The instability results were predominantly positive, with only one area plot for 0,5 deformation. At the deformation of 0,2, the instability results are similar to those of the deformation of 0,5, at the deformation of 0,8 there was any ξ value as negative.

CONCLUSIONS

The introduction describes the mathematics of detecting dissipation and instability in the forming process. In describing the behavior of the material, especially at high forming temperatures, the classical Sellars-Tegart-Garofalo method is used, which gradu-

ally derives constants n, β, α using linear regression analyzes and gradually searches constants into the final equation (sinh) (11). Comparing the stress peaks found experimentally σ_{pex} with the calculated $\sigma_{pca\ 1}$ gives a very good match. This relationship allows to predict with high accuracy the behavior of the material at different temperatures and strain rates than the experimental values. Similarly, through a sinh relationship, another general equation for deformations at the peak was derived (14). Here again, the agreement of experimental ε_{pex} and calculated values ε_{pca} is shown.

The last equation (15) was not used, since the material shows a minimal decrease behind the peak and even difficult to determine at high rate of deformation of 100 s^{-1} in the experiment. Since the stress with temperature behaves generally according to the Arhenius exponential relation, the stress peaks were calculated and are listed in the column in the table as $\sigma_{pca\ 2}$. We also extrapolated from the original four strain rates of 1 to 100 s^{-1} to values of 0,01 s^{-1} and 500 s^{-1} and in the table are recorded in gray rows. Here, especially for the prediction at 500 s^{-1}, the calculated stress values seem reasonable, while the peak distortions are more divergent. However, only experimental results at 0,2, 0,5 and 0,8 strains were used for further calculations of dissipation and instability.

Dissipation values η do not differ significantly with different strains; higher values are expected to occur at higher temperatures. It appears that the investigated medium medium-carbon steel does not play any significant changes in the energy dissipation despite the gradual dynamic recrystallization at lower temperatures and higher strain rates. This is also reflected in instability, quite surprisingly, we did not get negative values with the instability parameter ξ of 0.8 strain. A temperature range of 950°C to 1050°C and a low rate of deformation appear to be the most problematic.

REFERENCES

1. Y.V.R.K. Prasad, S. Sasidhara, Hot Working Guide: Compendium of Processing Maps, ASM International, 1997.
2. X. Gao, Z. Jiang, D. Wei, S. Jiao, D. Chen, Study on hot-working behavior of high carbon steel / low carbon steel composite material using processing map, Key Eng. Mater., 622-623, 2014, 330-339.
3. Y.V.R.K. Prasad, K.P. Rao, Processing maps for hot deformation of rolled AZ31 magnesium alloy plate: Anisotropy of hot workability, Materials Science And Engineering A, 487, 2008, 316-327.
4. N. Srinivasan, Y.V.R.K. Prasad, P. Rama Rao, Hot deformation behaviour of Mg-3Al alloy - A study using processing map, Materials Science And Engineering A, 476, 2008, 146-156.
5. Guoliang Ji , Fuguo Li , Qinghua Li , Huiqu Li, Zhi Li, Development and validation of a processing map for Aermet100 steel, Materials Science and Engineering A, 527, 2010, 1165-1171.
6. H. Li, M.Q. Li, X.Y. Zhang, J. Luo, Characterization of the forgeability of1Cr11Ni2W2MoV steel using processing map, Materials Science and Engineering A, 527, 2010, 6505-6510.
7. H.Y. Kim, H.C. Kwon, H.W. Lee, Y.T. Im, S.M. Byon, H.D. Park, Processing map approach for surface defect prediction in the hot bar rolling. Journal of Materials Processing Technology, 205, 2008, 70-80.
8. G.Z. Quan, Z.Y. Zou, T. Wang, B. Liu, J.C. Li, Modeling the Hot Deformation Behaviors of As-Extruded 7075 Aluminum Alloy by an Artificial Neural Network with Back-Propagation Algorithm, High Temp. Mater. Processes, 36, 2017, 1-13.
9. Z. Gronostajski, Constitutive equations for FEM analysis, J. Mater. Process. Technol., 106, 2000, 40-44.
10. A.K.S.K. Kumar, Master's Thesis, Bangalore: Indian Institute of Science, 1987.
11. Y.V.R.K. Prasad, Recent advances in the science of mechanical processing, Indian J. Technol., 28, 1990, 435-451.
12. H. Ziegler, Progress in Solid Mechanics. Vol 4, New York: John Wiley and Sons, 1963.
13. N. Yongquan, Y. Zekun, G. Hongzhen, M.W. Fub, L. Hui, X. Xiea, Investigation on hot deformation behavior of P/M Ni-base superalloy FGH96 by using processing maps, Materials Science and Engineering A, 527, 2010, 6794-6799.
14. W. Kai, L. Guoquan, H. Benfu, L. Feng, Z. Yiwen, T. Yu, L. Jiantao, Characterization of hot deformation behavior of a new Ni–Cr–Co based P/M superalloy, Materials characterization, 61, 2010, 330-340.
15. J. Kliber, I. Schindler, Stress-Strain Curves Computer Modelling of Deformed Steels at Elevated Temperatures. 9th International Conference on the Strength of Metals and Alloys, Haifa, Israel, 14-19 July 1991, 647-654.

16. J. Kliber, New approaches in describing stress-strain curves, Inter. Conf. Formability, Ostrava 1994, 77-83.
17. J. Kliber, I. Schindler, Mathematical description of Stress-Strain Curve in Metal Forming Processes, Metalurgija, 35, 2, 1996, 108.
18. J. Kliber, Torsion Test and its Evaluation, Int. Symp. 13 th IFHTSE/ASM Surface Engineering Congress, Columbus, Ohio, October 2002, 290-295.
19. A. Cingara, H. J. McQueen, New formula for calculating flow curves from high temperature constitutive data for 300 austenitic steels, J. Mater. Process. Technol., 36, 1992, 31-42.
20. H.J. McQueen, N. Jin, N.D. Ryan, Relationship of energy dissipation efficiency to microstructural evolution in hot working of AISI 304 steel. Materials Science and Engineering A, 190, 1995, 43-53.
21. Y.V.R.K. Prasad, H.L. Gegel, S.M. Doraivelu, J.C. Malas, J.T. Morgan, K.A. Lark, D.R. Barker, Modeling of dynamic material behavior in hot deformation: Forging of Ti-6242, Metall. Trans. A, 15, 1984, 1883-1892.
22. H.L. Gegel, J.C. Malas, S.M. Doraivelu, V.A. Shende, Metals Handbook, 9th ed., ASM, Metals Park, 14, 1988, 417-438.
23. J. M. Alexander, Mapping Dynamic Material Behaviour, Modelling Hot Deformation of Steels, Berlin: Springer-Verlag, 1989, 101-115.
24. G.Z. Quan, L. Zhao, T. Chen, Y. Wang, Y.P. Mao, W.Q. Lv, J. Zhou, Identification for the optimal working parameters of as-extruded 42CrMo high-strength steel from a large range of strain, strain rate and temperature, Mater. Sci. Eng. A, 538, 2012, 364-373.
25. P. Sonnek, J. Petruželka, The use of processing maps for prediction of metalflow stability in hot forming, 10th International Metallurgical and Materials Conference (METAL-2001), Ostrava: Tanger Ltd, 2001, 142.
26. J. Kliber, Computer simulation of hot forming efficiency, Int. Conference Machine-Building and Technosphere at the Boundary of the XXI Century, 10-15 September 2001 Sevastopol, Ukraine, 144-148.
27. P. Opěla, I. Schindler, P. Kawulok, F. Vančura, R. Kawulok, S. Rusz, T. Petrek, Hot flow stress models of the steel c45, Metalurgija, 54, 2015, 469-472.
28. P. Opěla, I. Schindler, P. Kawulok, F. Vančura, R. Kawulok, S. Rusz, New model predicting flow curves in wide range of thermomechanical conditions of 38MnVS6 steel, 25th Anniversary International Conference on Metallurgy and Materials (METAL-2016), Ostrava: Tanger Ltd, 2016, 458-463.
29. J. Kliber, Počítačová simulace účinnosti při tváření za tepla - část I. In. Mez. věd konference "Forming 97", Hotel Relax, Rožnov pod Radhoštěm, VŠB-TU Ostrava a Polit. Slaska Katowice, 1997, 61-65 (in Czech).
30. J. Kliber, Dissipation of energy and instability process in various alloys based on plastometric tests, Materials Physics and Mechanics, 25, 2016, 16-21.
31. P. Opěla, I. Schindler, S. Rusz, P. Kawulok, R. Kawulok, V. Ševčák, Possibilities of Assembling of Processing Maps by Utilizing of an Artificial Neural Network Approach. IOP Conference Series: Materials Science and Engineering, 461(1), 2019, Article number: 012063.